Ockeloen-Korppi, Caspar; Damskägg, Erno; Pirkkalainen, Juha-Matti; Heikkilä, T. T.; Massel, Francesco; Sillanpää, Mika

Low-Noise Amplification and Frequency Conversion with a Multiport Microwave Optomechanical Device

Published in:
Physical Review X

DOI:
10.1103/PhysRevX.6.041024

Published: 28/10/2016

Document Version
Publisher's PDF, also known as Version of record

Low-Noise Amplification and Frequency Conversion with a Multiport Microwave Optomechanical Device

C. F. Ockeloen-Korppi,[1] E. Damskägg,[1] J.-M. Pirkkalainen,[1] T. T. Heikkilä,[2] F. Massel,[2] and M. A. Sillanpää[1,*]

[1]*Department of Applied Physics, Aalto University, P.O. Box 11100, FI-00076 Aalto, Finland*

[2]*Department of Physics, Nanoscience Center, University of Jyvaskyla, P.O. Box 35 (YFL), FI-40014 University of Jyvaskyla, Finland*

(Received 20 June 2016; revised manuscript received 22 September 2016; published 28 October 2016)

High-gain amplifiers of electromagnetic signals operating near the quantum limit are crucial for quantum information systems and ultrasensitive quantum measurements. However, the existing techniques have a limited gain-bandwidth product and only operate with weak input signals. Here, we demonstrate a two-port optomechanical scheme for amplification and routing of microwave signals, a system that simultaneously performs high-gain amplification and frequency conversion in the quantum regime. Our amplifier, implemented in a two-cavity microwave optomechanical device, shows 41 dB of gain and has a high dynamic range, handling input signals up to 10^{13} photons per second, 3 orders of magnitude more than corresponding Josephson parametric amplifiers. We show that although the active medium, the mechanical resonator, is at a high temperature far from the quantum limit, only 4.6 quanta of noise is added to the input signal. Our method can be readily applied to a wide variety of optomechanical systems, including hybrid optical-microwave systems, creating a universal hub for signals at the quantum level.

DOI: 10.1103/PhysRevX.6.041024 Subject Areas: Quantum Physics

Recent advances in near-quantum-limited amplifiers in the microwave-frequency regime have led to breakthroughs in the understanding of quantum measurement processes [1–4] and are necessary in quantum error correction and feedback [5–7]. Of particular interest for most applications are phase-insensitive linear amplifiers, which provide a faithful reconstruction of both quadratures of the input. Such amplifiers are bound by the standard quantum limit (SQL), which states that at high gain at least half an energy quantum of noise is added to the input signal [8]. This limit has been approached with Josephson parametric amplifiers [9–14]; however, such amplifiers are limited to relatively weak input signals. Optomechanical amplifiers or detectors, utilizing the interaction between electromagnetic waves and a mechanical resonator inside a cavity [15], have been demonstrated in the microwave and optical regime [16–19], but existing techniques suffer from a limited gain and bandwidth as well as noise levels well above the SQL.

In this paper, we demonstrate a two-port optomechanical device, motivated by the proposal in Ref. [20]. It consists of two electromagnetic cavities with different resonant frequencies, simultaneously coupled [21–23] to a single mechanical resonator. In the presence of appropriately chosen external pump tones, the mechanical resonator mediates interaction between the cavities, enabling strong amplification of a signal reflected from one of the cavities. Moreover, the scheme supports frequency-converting amplification, where a signal incident in one cavity can irradiate out from the other cavity at a completely different frequency, while being amplified at the same time. As we show theoretically, our scheme can reach the SQL for both of these processes. Unlike existing optomechanical amplifiers [16,17], the bandwidth of amplification in our scheme can be in principle increased up to the cavity linewidth, and the product of gain and bandwidth has no fundamental limit. Remarkably, we show in experiment that the quantum limit can be closely approached even at a high temperature where the mode occupation numbers $\gg 1$, which allows for an interpretation in terms of reservoir engineering [20,24–27].

In a microwave-frequency optomechanical [28] experiment, we obtain a gain of 41 dB with a gain-bandwidth product of 137 kHz, while adding only 4 quanta of noise above the SQL. Additionally, we show how the multimode system can act as a spectrally pure microwave source in the regime of self-oscillations. Finally, using an alternate pump scheme, our system also supports frequency conversion without amplification, similar to previous experiments in a range of systems [22,23,29,30]. With that method, we observe near-unity conversion efficiency, wide bandwidth, and added noise on the single photon level.

Our setup is shown in Fig. 1 and discussed in detail in the Supplemental Material [31]. At the heart of our device is a suspended aluminium drum resonator [3], with a resonant frequency of $\omega_m = 2\pi \times 8.3$ MHz and a linewidth of

*mika.sillanpaa@aalto.fi

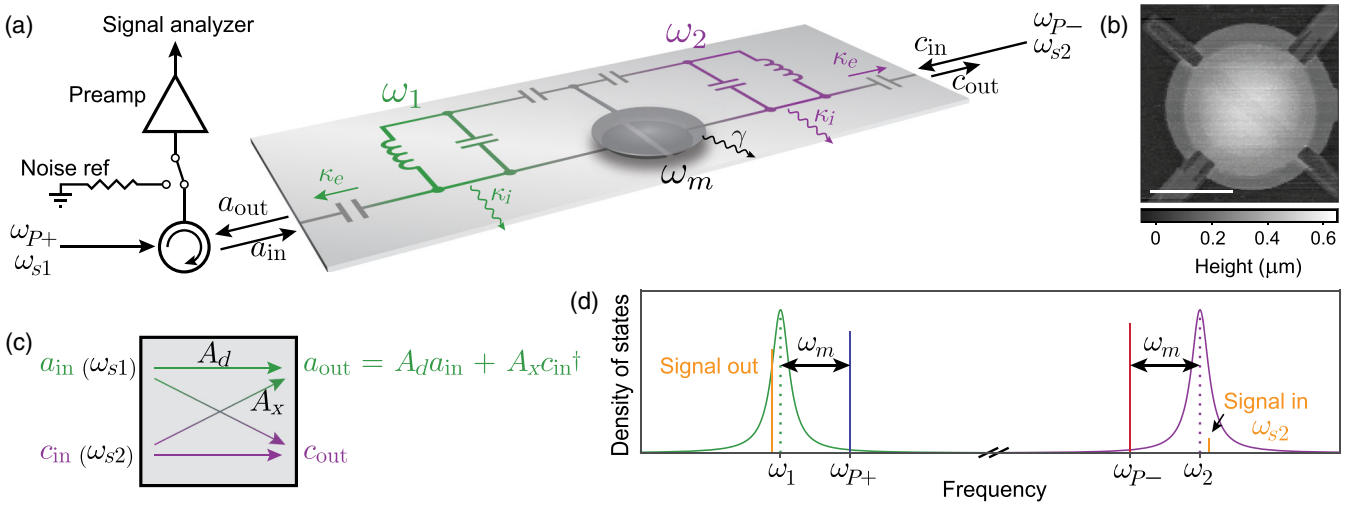

FIG. 1. Experimental setup. (a) Schematic of our device, showing two LC microwave cavities (ω_1, ω_2) both coupled to a central mechanical drum resonator (ω_m) as well as an individual feed line. Signals (ω_{s1}, ω_{s2}) and pumps (ω_{P+}, ω_{P-}) are fed to the cavities as shown. The output of cavity 1 is preamplified and measured with a signal analyzer. (b) Atomic force micrograph of the drum resonator. Scale bar is 10 μm long. (c) Conceptual two-port amplifier, exhibiting both direct (A_d) and cross (A_x) gain. (d) Schematic representation of the cavity modes and pump frequencies used to realize a two-port amplifier. As an example, an input signal with frequency ω_{s2} is injected to cavity 2, with the frequency-converted and amplified output emerging from cavity 1.

$\gamma = 2\pi \times 100$ Hz, fabricated on a quartz substrate. The drum is surrounded by two inductor-capacitor (LC) cavities, with resonant frequencies $\omega_1 = 2\pi \times 7.0$ GHz and $\omega_2 = 2\pi \times 8.4$ GHz, respectively. The mechanical resonator is suspended over two electrodes to form a variable capacitance in each cavity, simultaneously coupling the mechanical motion to both cavities. Each cavity is capacitively coupled to an individual transmission line with a strong coupling rate, $\kappa_e = 2\pi \times 4.8$ MHz, compared to the internal loss rate, $\kappa_i = 2\pi \times 0.50$ MHz. The total cavity linewidth is $\kappa = \kappa_i + \kappa_e$.

The two-mode amplifier is created by injecting two pump tones [Fig. 1(d)], one at the blue mechanical sideband of cavity 1 ($\omega_{P+} = \omega_1 + \omega_m$), and the other at the red sideband of cavity 2 ($\omega_{P-} = \omega_2 - \omega_m$). In the presence of strong pump tones, the optomechanical interaction is effectively linear and enhanced by the cavity, with coupling strengths $G_+ = \sqrt{n_1} g_1$ and $G_- = \sqrt{n_2} g_2$, where g_i is the single-photon coupling strength and n_i the photon occupation of cavity i. We also define $\mathcal{G}^2 = (G_-^2 - G_+^2)$ and the effective damping $\gamma_{\rm eff} = \gamma + 4\mathcal{G}^2/\kappa$ of the mechanical resonator. Quantum-limited amplification in related multicavity configurations have been theoretically proposed [20,32,33]. Reference [20] treats a special case of equal pump tones, $G_- = G_+$, whereas Ref. [32] discusses an inverted dissipation hierarchy, where the linewidth of the mechanical resonator is much larger than κ. The latter case, using cavity damping to enhance γ, was experimentally realized in a work simultaneous to ours [34]. In our work, we treat the case $G_- \gtrsim G_+$ and $\gamma_{\rm eff} \ll \kappa$. Moreover, we introduce the possibility for frequency-converting amplification, in addition to unity-gain frequency conversion [22,23,29,30].

The effective Hamiltonian describing the coupling between the subsystems is

$$H_I = (G_- c^\dagger + G_+ a) b + \text{H.c.} \tag{1}$$

($\hbar = 1$ hereafter), where the operators a, $a^\dagger$ and c, $c^\dagger$ represent cavity 1 and 2, respectively, and b, $b^\dagger$ represent the mechanical mode. H_I can be interpreted as a two-step process composed of nondegenerate parametric amplification [1,35] between cavity 1 and the mechanics (term $G_+ ab + \text{H.c.}$), followed by a beam splitter between the mechanics and cavity 2 (term $G_- c^\dagger b + \text{H.c.}$), which acts as a means to transfer the amplification to cavity 2.

Using input-output theory, and assuming $G_- \gtrsim G_+$, we find the system behaves as a two-port phase-insensitive linear amplifier, as depicted schematically in Fig. 1(c). The output field $a_{\rm out}$ of cavity 1 has the from

$$a_{\rm out} = A_d a_{\rm in} + A_x c_{\rm in}^\dagger + F, \tag{2}$$

and similar for $c_{\rm out}$ of cavity 2. Here, A_d is the direct gain of signals $a_{\rm in}$ incident on cavity 1 and A_x is the cross (frequency-converting) gain of signals incident on cavity 2. Operator F describes the added noise due to the internal modes of the device, viz. $\mathcal{G}^2 \ll G_-^2$. In this case, the direct and cross gains are approximately equal, with peak values on resonance

$$|A_d|^2 \approx |A_x|^2 \approx \left|2\frac{\kappa_e}{\kappa}\frac{4G_-^2/\kappa}{\gamma_{\rm eff}}\right|^2. \quad (3)$$

Similar to optomechanical amplifiers powered by a single blue-detuned pump [16], the amplification bandwidth is associated with the effective mechanical linewidth $\gamma_{\rm eff}$. In the present case, however, the parametric instability threshold is not reached as long as $\gamma_{\rm eff} > 0$ (see Ref. [27]), and further, the bandwidth can be increased beyond the intrinsic linewidth γ, in principle up to the onset of mode splitting $\gamma_{\rm eff} \simeq \kappa$ [20]. Moreover, the gain-bandwidth product, GBW $= |A_d|\gamma_{\rm eff}$, is determined by $G_- \approx G_+$, and is not fundamentally limited outside the mode-splitting region. The latter, however, can be fully controlled by $\mathcal{G}$, and, thus, the GBW is rigorously unlimited in the limiting case $G_- = G_+$.

To characterize the noise performance, we calculate the expected output noise power-spectral density (PSD), $S_{\rm out} = \frac{1}{2}\langle a_{\rm out}^\dagger a_{\rm out} + a_{\rm out}a_{\rm out}^\dagger\rangle$, from Eq. (2) (and similar for $c_{\rm out}$). The input-referred added noise is then calculated as $S_{\rm add} = (S_{\rm out} - S_{\rm in})/|A|^2$, where A is A_d or A_x for direct and frequency-converting amplification, respectively, and $S_{\rm in} = 1/2$ is vacuum input noise driving both cavities. In principle there could also be thermal input noise entering via the ports, but this is typically negligible. In the regime $\gamma\kappa/4 \ll \mathcal{G}^2 \ll G_-^2$ (that is, in the case of high gain and significantly broadened $\gamma_{\rm eff}$), the added noise for direct amplification can be expressed as [31]

$$S_{\rm add} \approx \frac{\gamma\kappa}{4G_-^2}\frac{\kappa}{\kappa_e}\left(n_m^T + \frac{1}{2}\right) + \frac{\kappa_i}{\kappa_e}(n_a^T + n_c^T + 1) + \frac{1}{2}. \quad (4)$$

Here, the first term originates from the thermal environment of the mechanical oscillator, with an effective temperature $T_{\rm env}$ corresponding to an occupation $n_m^T \approx k_B T_{\rm env}/\hbar\omega_m$. The second term corresponds to the thermal environment of the cavities, with thermal occupation numbers n_a^T and n_c^T for cavity 1 and 2, respectively. Finally, the last term is the vacuum noise of cavity 2. For large G_- and G_+, strong external coupling $\kappa_e \gg \kappa_i$, and narrow intrinsic mechanical linewidth such that $\gamma\kappa/4 \ll G_-^2$, the added noise approaches the quantum limit of one-half quantum. These conditions are available in realizations using either microwave or optical cavities. The fundamental quantum noise is effectively set by cavity 2 (the mode which is not the input). Importantly, the added noise due to the mechanical thermal environment is reduced by a cooperativity-like factor $\gamma\kappa/(4G_-^2)$. Hence, the quantum limit can be nearly reached even when the mechanical oscillator is at a high temperature, in stark contrast to the regular nondegenerate parametric amplifier [35].

Another figure of merit of an amplifier is the capability to handle large signal levels. Josephson parametric amplifiers operating near the quantum limit are poor in this regard. This is because the Josephson energy limits the energy stored in a single junction up to approximately 10^2 photons. Our approach is expected to show a clear improvement because it does not involve nonlinearities close to single-quantum energies. The limiting factor in our system is the critical current of aluminum, which typically allows 10^8 photons inside the cavity. Although Eq. (1) could be realized in Josephson junction systems as well, the large signal handling capabilities favor an electromechanical realization.

In experiment, we measure the performance of our amplifier in a cryogenic environment at a base temperature of 7 mK. We inject pumps and signals in both cavities, while measuring the output of cavity 1. Figure 2(a) shows the direct gain $|A_d|^2$, where the signal is injected into cavity 1. Data are shown as a function of signal frequency for $G_- = 2\pi \times$ 355 kHz and several values of G_+ up to $G_+ = 0.99G_-$, corresponding to the highest gain. We achieve a maximum gain of $|A_d|^2 = 41$ dB with a 3-dB bandwidth of $\gamma_{\rm eff} = 1.2$ kHz, resulting in GBW $= 137$ kHz. The data are in excellent agreement with fits to our model [31]. Figure 2(b) shows an example of frequency-converting

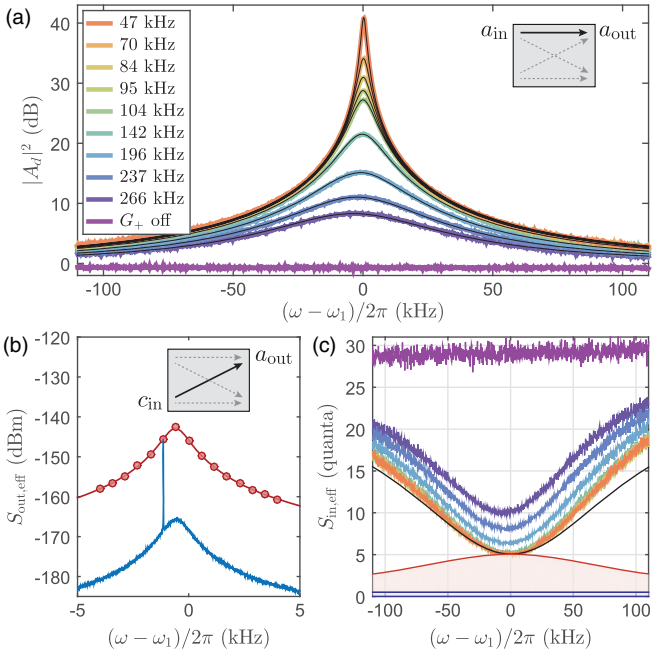

FIG. 2. Two-mode amplifier performance. (a) Direct gain $|A_d|^2$ versus signal frequency for fixed G_- and various values of G_+ (colored lines, legend shows $\mathcal{G}/2\pi$) together with theory fits (black lines). Inset: Amplifier configuration; the signal is input to cavity 1. (b) Example output spectrum of cavity 1 (blue line), showing high-gain frequency conversion of a weak signal injected in cavity 2 (narrow peak). The peak height at different frequencies (circles) agrees with the fitted model (red line). Inset: Amplifier configuration. (c) Effective input-referred noise for the same G_-,G_+ as in (a) (colored lines). The theory model (black line) is plotted only for the highest gain. The blue shaded area shows the input noise of one-half quanta at each input, and the red shaded area shows the modeled added noise $S_{\rm add}$.

amplification. Shown is the output spectrum of cavity 1, while a weak sinusoidal signal is injected into cavity 2 close to resonance, for $G_- \approx 2\pi \times 140$ kHz and $\mathcal{G} \approx 2\pi \times 40$ kHz. The converted output signal is visible as a narrow peak. The peak output is measured for several frequencies (circles), and the peak gain is $|A_x|^2 \approx 26$ dB.

To accurately quantify the noise performance, we calibrate the total system gain with two independent methods (see also Ref. [31]). First, we compare to a resistor with known 2.9-K thermal noise at the output side of the sample [Fig. 1(a)]. Second, in a subsequent cooldown, we verify the calibration with a tunable noise source at the input side of our sample. Using the latter method, we do not need to know the cable attenuation between the sample and the preamplifier. Using this calibration, we measure the effective noise $S_{\mathrm{out,eff}}$ at the sample output. Figure 2(c) shows the effective input-referred noise spectrum, $S_{\mathrm{in,eff}} = S_{\mathrm{out,eff}}/|A_d|^2$, with no signal input, expressed as number of quanta per unit bandwidth and regarding cavity 1 as the input port. $S_{\mathrm{in,eff}}$ is the total system noise: it consists of the input vacuum noise $S_{\mathrm{in}} = 1/2$ (blue shaded area), the added noise S_{add} of the mechanical amplifier (red shaded area), as well as the output technical noise $S_{H,\mathrm{eff}}$ added by all further amplification stages [31]. The latter dominates off resonance, but is negligible at high gain. The measured effective noise therefore reduces at increasing gain, saturating at $S_{\mathrm{in,eff}} \simeq 5$ quanta for $|A_d|^2 \gtrsim 20$ dB. This corresponds to an added noise of $S_{\mathrm{add}} = 4.6 \pm 1.0$ quanta at the highest gain measurement. The same result applies to frequency-converting amplification (with cavity 2 as the input port), since at high gain $|A_x| \approx |A_d|$. The uncertainty of S_{add} is dominated by the residual power calibration uncertainty.

In Figs. 3(a)–3(c), we summarize the performance of our amplifier for a wide range of pump powers. For fixed G_-, the gain-bandwidth product is approximately independent of $\mathcal{G}$, as expected from our model. The highest GBW $=$ 137 kHz as well as the highest absolute gain are achieved at highest G_-, which is, in turn, limited only by the experimentally available pump power. The optimal bandwidth, while maintaining a total system noise of 5 quanta, is $\gamma_{\mathrm{eff}} = 2\pi \times 11$ kHz, measured at a gain of 21.5 dB. Figure 3(c) shows the total input-referred noise $S_{\mathrm{in,eff}}$ on resonance, as well as the added noise S_{add} of our amplifier. At low pump powers, and thus low gain, we observe added noise below 2 quanta, but for high pump powers, S_{add} increases. Comparing to our theory model, we find that the noise performance is well described by heating of the mechanical environment at high pump powers, up to $n_m^T \approx 5 \times 10^3$ quanta. These results are consistent with the heating we observe with standard optomechanical cooling measurements [31]. While heating processes limit the noise performance of the current experiment, they do not pose a fundamental limit on our scheme. The heating could be reduced by increased optomechanical couplings g_1 and g_2 and improved mechanical and cavity quality factors, and further depends on the details of device fabrication.

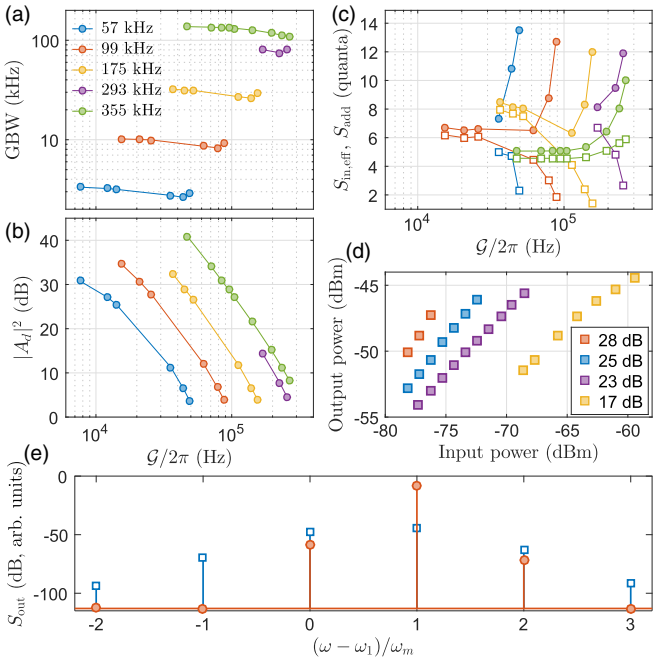

FIG. 3. Amplifier performance and oscillations. (a) Gain-bandwidth product for several values of G_- (legends show $G_-/2\pi$) as a function of $\mathcal{G}$. (b) Peak direct gain and (c) effective input-referred noise (closed circles) and added amplifier noise S_{add} (open squares) on resonance, for the same parameters as (a). (d) Performance of direct amplification at large input powers, measured for $G_- \approx 2\pi \times 350$ kHz and several values of $\mathcal{G}$ (colors). Legend shows the nominal gain for each setting. (e) Harmonic spectra of oscillations in the instability regime without (open squares) and with (closed circles) the red-detuned pump at ω_{P-} enabled. For the latter case, each harmonic component is measured separately and the horizontal line shows the measurement noise floor.

In addition to operating the pump frequencies at sideband coresonance, our amplifier can be tuned over the cavity linewidth κ by shifting the pump frequencies. We measure high-gain ($|A_d|^2 > 26$ dB) and low-noise ($S_{\mathrm{in,eff}} \approx 5$ quanta) amplification over a tuning range of 2 MHz. Further tuning could be achieved with tunable microwave cavities [36]. Free-space optical cavities, which have been used in optomechanical systems [15], directly provide tuning over a wide range.

In contrast to existing amplifiers operating near the quantum limit, our amplifier can handle large signal levels. Figure 3(d) shows the output power versus input power, as measured at the sample port, for several nominal gain settings and for the largest input powers where the system remains stable. With a gain of 23 dB and similar pump powers as in Fig. 2, our amplifier remains stable up to an input power of -69 dBm, or 3×10^{13} photons/s. This is 30 dB higher than reported in Josephson parametric amplifiers [14], and corresponds to a very large dynamic range of 127 dB in a 1-Hz measurement bandwidth. In these large-signal measurements, the signal-to-noise ratio

(SNR) is > 100 dB in a 1-Hz measurement bandwidth, limited by the phase noise of our signal generator. Since we see no evidence of increased noise towards higher input powers, we believe the SNR is equal to the dynamic range, which is 5 orders of magnitude higher than in typical Josephson parametric amplifiers [10], and comparable to the highest values obtained with nearly quantum-limited microwave measurement systems [37].

When increasing G_+ beyond the stability requirement $\gamma_{\rm eff} > 0$, the system undergoes a lasing transition to self-sustained oscillations, which can be a source of spectrally pure electromagnetic radiation [32]. Figure 3(e) shows the measured harmonic spectrum of such oscillations for the two-cavity case (both pumps ω_{P+} and ω_{P-} on) and for the case of a single pump ω_{P+}. Whereas the single pump case shows many harmonic components, in the two-cavity case we observe only a single sideband at $\pm\omega_m$ around the pump frequency ω_{P+}. The absence of higher sidebands demonstrates that the mechanical resonator has pure sinusoidal oscillations, which can allow for applications as a source of a clean clock signal.

In a third experiment, we demonstrate coherent frequency conversion of microwave signals without amplification, a frequency-converting analog to an optical beam splitter. This method has been previously demonstrated with optical frequencies [22,23], hybrid microwave-optical systems [29], and very recently in a system similar to ours [30]. Both cavities are pumped at the red mechanical sideband, with pump frequencies $\omega_{Pi} = \omega_i - \omega_m$ for cavity $i = 1, 2$, respectively. A weak input signal with frequency ω_s is injected into cavity 2. The converted signal appears at the output of cavity 1, with a frequency $\omega_s' = \omega_s - \omega_{P2} + \omega_{P1}$. The internal conversion efficiency between the two cavities is [22]

$$\eta_{\rm int} = \frac{4G_1^2G_2^2}{(G_1^2 + G_2^2 + \frac{\gamma\kappa}{4})^2}, \tag{5}$$

which approaches unity for $G_1^2 = G_2^2 \gg (\gamma\kappa/4)$. Here, $G_i = \sqrt{n_i}g_i$. The total conversion efficiency from input to output is $\eta = \eta_{\rm int}\kappa_e^2/\kappa^2$.

The experimental results are shown in Fig. 4. Figure 4(a) shows the output power spectral density $S(\omega')$ for several input frequencies close to ω_2. The output signal is visible as a narrow peak. The conversion has a bandwidth of 50 kHz, corresponding to the mechanical linewidth broadened by optomechanical cooling by both pumps. Figure 4(c) shows the maximum internal conversion efficiency at $\omega_s = \omega_2$ as a function of output-cavity pump power P_{P1}, for various input-cavity pump powers P_{P2}, together with a global fit of all the data to Eq. (5). We obtain a peak internal efficiency of $\eta_{\rm int} > 0.99$, and the total efficiency is limited only by the cavity coupling $\eta \approx \kappa_e^2/\kappa^2 \gtrsim 0.82$. Similar to the two-port amplifier, we observe an increase in noise due to heating of the mechanics at the highest pump powers, resulting in an

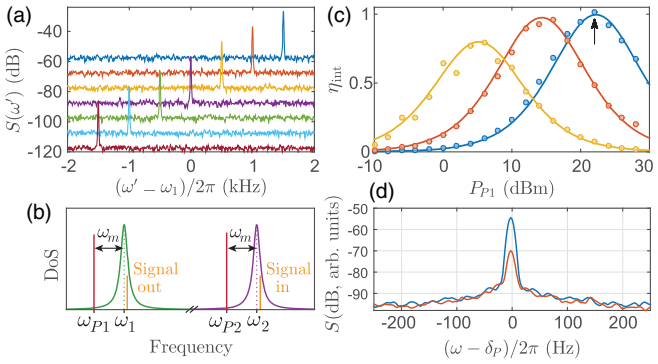

FIG. 4. Frequency conversion without amplification. (a) Output spectrum $S(\omega')$ (arbitrary units, each curve offset by 10 dB) showing the frequency-converted output signal $\omega_s' \approx \omega_1$ for several input frequencies $\omega_s \approx \omega_2$. (b) Pump and signal configuration. (c) Conversion efficiency on resonance ($\omega_s = \omega_2$) along with fitted theory (see text), for $P_{P2} \approx 4$ dBm (yellow), 14 dBm (red), and 22 dBm (blue), in the same units as P_{P1}. Arrow indicates data shown in (a). (d) Coherence of conversion. Shown are spectra of the mixed-down pump tone δ_P (blue line) and the destructive interference of δ_P and δ_s (red line).

added noise of 3.9 quanta at near-unity conversion efficiency. Using lower pump powers, we obtain an added noise of 1.4 quanta, while retaining a conversion efficiency of $\eta_{\rm int} = 0.95$. In optical and hybrid systems, much lower efficiencies have been reached, mostly limited by κ_e [22,23,29]. To verify coherence of the conversion process, we externally mix the input and output signals, generating their difference frequency $\delta_s = \omega_s - \omega_s'$. Similarly, we mix together the two probe tones to generate $\delta_P = \omega_{P2} - \omega_{P1}$. We then combine δ_s and δ_P on a resistive adder, and with appropriately adjusted relative phase and amplitude we observe 15 dB of destructive interference between the two tones, as shown in Fig. 4(d). We thus demonstrate coherent frequency conversion near the quantum limit.

Our concept of a two-port optomechanical phase-insensitive amplifier can be readily applied to other optomechanical systems which have been recently demonstrated, including optical [22,23] and hybrid optical-microwave systems [29], providing an essential link to create hybrid networks of otherwise incompatible quantum systems [38–40]. Extending our scheme to multiple cavity modes creates a universal hub for electromechanical or optomechanical signals at the quantum level [41,42], with high-gain, high-power amplification enabling interconnection of remote systems. At optical frequencies [43], the quantum limit of added noise should be accessible at room temperature. Given that in the present microwave experiment the added noise is limited by residual heating of the mechanical resonator, we expect the quantum limit can be reached by, first of all, improving the coupling efficiency. With a factor of 2 higher coupling, and an order of magnitude higher pump powers feasible, in particular, in 3D cavities [44] with niobium technology, the device can

operate at MHz-range bandwidth close to the standard quantum limit at 4-K temperatures, hence presenting an attractive alternative to HEMT amplifiers in narrow-band microwave measurements.

We thank Visa Vesterinen and Pasi Lähteenmäki for useful discussions. This work was supported by the Academy of Finland (Contract No. 250280, CoE LTQ, 275245) and by the European Research Council (240387-NEMSQED, 240362-Heattronics, 615755-CAVITYQPD). The work benefited from the facilities at the Micronova Nanofabrication Center and at the Low Temperature Laboratory infrastructure.

C. F. O.-K. carried out the practical work, analyzed data, and wrote the paper. E. D. and J.-M. P. developed the device fabrication process. T. T. H. and F. M. developed the theory. M. A. S initiated and supervised the project.

[1] A. A. Clerk, M. H. Devoret, S. M. Girvin, F. Marquardt, and R. J. Schoelkopf, *Introduction to Quantum Noise, Measurement, and Amplification*, Rev. Mod. Phys. **82**, 1155 (2010).

[2] R. Vijay, D. H. Slichter, and I. Siddiqi, *Observation of Quantum Jumps in a Superconducting Artificial Atom*, Phys. Rev. Lett. **106**, 110502 (2011).

[3] J. D. Teufel, T. Donner, D. Li, J. W. Harlow, M. S. Allman, K. Cicak, A. J. Sirois, J. D. Whittaker, K. W. Lehnert, and R. W. Simmonds, *Sideband Cooling of Micromechanical Motion to the Quantum Ground State*, Nature (London) **475**, 359 (2011).

[4] L. Steffen, Y. Salathe, M. Oppliger, P. Kurpiers, M. Baur, C. Lang, C. Eichler, G. Puebla-Hellmann, A. Fedorov, and A. Wallraff, *Deterministic Quantum Teleportation with Feed-Forward in a Solid State System*, Nature (London) **500**, 319 (2013).

[5] R. Vijay, C. Macklin, D. H. Slichter, S. J. Weber, K. W. Murch, R. Naik, A. N. Korotkov, and I. Siddiqi, *Stabilizing Rabi Oscillations in a Superconducting Qubit Using Quantum Feedback*, Nature (London) **490**, 77 (2012).

[6] J. Kelly *et al.*, *State Preservation by Repetitive Error Detection in a Superconducting Quantum Circuit*, Nature (London) **519**, 66 (2015).

[7] D. J. Wilson, V. Sudhir, N. Piro, R. Schilling, A. Ghadimi, and T. J. Kippenberg, *Measurement-Based Control of a Mechanical Oscillator at Its Thermal Decoherence Rate*, Nature (London) **524**, 325 (2015).

[8] C. M. Caves, *Quantum Limits on Noise in Linear Amplifiers*, Phys. Rev. D **26**, 1817 (1982).

[9] B. Yurke, L. R. Corruccini, P. G. Kaminsky, L. W. Rupp, A. D. Smith, A. H. Silver, R. W. Simon, and E. A. Whittaker, *Observation of Parametric Amplification and Deamplification in a Josephson Parametric Amplifier*, Phys. Rev. A **39**, 2519 (1989).

[10] M. A. Castellanos-Beltran, K. D. Irwin, G. C. Hilton, L. R. Vale, and K. W. Lehnert, *Amplification and Squeezing of Quantum Noise with a Tunable Josephson Metamaterial*, Nat. Phys. **4**, 929 (2008).

[11] N. Bergeal, F. Schackert, M. Metcalfe, R. Vijay, V. E. Manucharyan, L. Frunzio, D. E. Prober, R. J. Schoelkopf, S. M. Girvin, and M. H. Devoret, *Phase-Preserving Amplification Near the Quantum Limit with a Josephson Ring Modulator*, Nature (London) **465**, 64 (2010).

[12] P. Lähteenmäki, V. Vesterinen, J. Hassel, H. Seppä, and P. Hakonen, *Josephson Junction Microwave Amplifier in Self-Organized Noise Compression Mode*, Sci. Rep. **2**, 276 (2012).

[13] C. Eichler, Y. Salathe, J. Mlynek, S. Schmidt, and A. Wallraff, *Quantum-Limited Amplification and Entanglement in Coupled Nonlinear Resonators*, Phys. Rev. Lett. **113**, 110502 (2014).

[14] C. Macklin, K. O'Brien, D. Hover, M. E. Schwartz, V. Bolkhovsky, X. Zhang, W. D. Oliver, and I. Siddiqi, *A Near-Quantum-Limited Josephson Traveling-Wave Parametric Amplifier*, Science **350**, 307 (2015).

[15] M. Aspelmeyer, T. J. Kippenberg, and F. Marquardt, *Cavity Optomechanics*, Rev. Mod. Phys. **86**, 1391 (2014).

[16] F. Massel, T. T. Heikkilä, J.-M. Pirkkalainen, S. U. Cho, H. Saloniemi, P. J. Hakonen, and M. A. Sillanpää, *Microwave Amplification with Nanomechanical Resonators*, Nature (London) **480**, 351 (2011).

[17] T. G. McRae and W. P. Bowen, *Near Threshold All-Optical Backaction Amplifier*, Appl. Phys. Lett. **100**, 201101 (2012).

[18] H. Li, Y. Chen, J. Noh, S. Tadesse, and M. Li, *Multichannel Cavity Optomechanics for All-Optical Amplification of Radio Frequency Signals*, Nat. Commun. **3**, 1091 (2012).

[19] T. Bagci, A. Simonsen, S. Schmid, L. G. Villanueva, E. Zeuthen, J. Appel, J. M. Taylor, A. Sorensen, K. Usami, A. Schliesser, and E. S. Polzik, *Optical Detection of Radio Waves through a Nanomechanical Transducer*, Nature (London) **507**, 81 (2014).

[20] A. Metelmann and A. A. Clerk, *Quantum-Limited Amplification via Reservoir Engineering*, Phys. Rev. Lett. **112**, 133904 (2014).

[21] I. S. Grudinin, H. Lee, O. Painter, and K. J. Vahala, *Phonon Laser Action in a Tunable Two-Level System*, Phys. Rev. Lett. **104**, 083901 (2010).

[22] C. Dong, V. Fiore, M. C. Kuzyk, and H. Wang, *Optomechanical Dark Mode*, Science **338**, 1609 (2012).

[23] J. T. Hill, A. H. Safavi-Naeini, J. Chan, and O. Painter, *Coherent Optical Wavelength Conversion via Cavity Optomechanics*, Nat. Commun. **3**, 1196 (2012).

[24] J. F. Poyatos, J. I. Cirac, and P. Zoller, *Quantum Reservoir Engineering with Laser Cooled Trapped Ions*, Phys. Rev. Lett. **77**, 4728 (1996).

[25] K. W. Murch, U. Vool, D. Zhou, S. J. Weber, S. M. Girvin, and I. Siddiqi, *Cavity-Assisted Quantum Bath Engineering*, Phys. Rev. Lett. **109**, 183602 (2012).

[26] S. Shankar, M. Hatridge, Z. Leghtas, K. M. Sliwa, A. Narla, U. Vool, S. M. Girvin, L. Frunzio, M. Mirrahimi, and M. H. Devoret, *Autonomously Stabilized Entanglement between Two Superconducting Quantum Bits*, Nature (London) **504**, 419 (2013).

[27] Y.-D. Wang and A. A. Clerk, *Reservoir-Engineered Entanglement in Optomechanical Systems*, Phys. Rev. Lett. **110**, 253601 (2013).

[28] C. A. Regal, J. D. Teufel, and K. W. Lehnert, *Measuring Nanomechanical Motion with a Microwave Cavity Interferometer*, Nat. Phys. **4**, 555 (2008).
[29] R. W. Andrews, R. W. Peterson, T. P. Purdy, K. Cicak, R. W. Simmonds, C. A. Regal, and K. W. Lehnert, *Bidirectional and Efficient Conversion between Microwave and Optical Light*, Nat. Phys. **10**, 321 (2014).
[30] F. Lecocq, J. B. Clark, R. W. Simmonds, J. Aumentado, and J. D. Teufel, *Mechanically Mediated Microwave Frequency Conversion in the Quantum Regime*, Phys. Rev. Lett. **116**, 043601 (2016).
[31] See Supplemental Material at http://link.aps.org/supplemental/10.1103/PhysRevX.6.041024 for details on the theoretical model, experimental setup, and data analysis.
[32] A. Nunnenkamp, V. Sudhir, A. K. Feofanov, A. Roulet, and T. J. Kippenberg, *Quantum-Limited Amplification and Parametric Instability in the Reversed Dissipation Regime of Cavity Optomechanics*, Phys. Rev. Lett. **113**, 023604 (2014).
[33] A. Metelmann and A. A. Clerk, *Nonreciprocal Photon Transmission and Amplification via Reservoir Engineering*, Phys. Rev. X **5**, 021025 (2015).
[34] L. D. Tóth, N. R. Bernier, A. Nunnenkamp, E. Glushkov, A. K. Feofanov, and T. J. Kippenberg, *Engineered Dissipative Reservoir for Microwave Light Using Circuit Optomechanics*, arXiv:1602.05180.
[35] W. H. Louisell, A. Yariv, and A. E. Siegman, *Quantum Fluctuations and Noise in Parametric Processes. I.*, Phys. Rev. **124**, 1646 (1961).
[36] R. W. Andrews, A. P. Reed, K. Cicak, J. D. Teufel, and K. W. Lehnert, *Quantum-Enabled Temporal and Spectral Mode Conversion of Microwave Signals*, Nat. Commun. **6**, 10021 (2015).
[37] B. H. Eom, P. K. Day, H. G. LeDuc, and J. Zmuidzinas, *A Wideband, Low-Noise Superconducting Amplifier with High Dynamic Range*, Nat. Phys. **8**, 623 (2012).
[38] Z.-L. Xiang, S. Ashhab, J. Q. You, and F. Nori, *Hybrid Quantum Circuits: Superconducting Circuits Interacting with Other Quantum Systems*, Rev. Mod. Phys. **85**, 623 (2013).
[39] J. Bochmann, A. Vainsencher, D. D. Awschalom, and A. N. Cleland, *Nanomechanical Coupling between Microwave and Optical Photons*, Nat. Phys. **9**, 712 (2013).
[40] G. Kurizki, P. Bertet, Y. Kubo, K. Mølmer, D. Petrosyan, P. Rabl, and J. Schmiedmayer, *Quantum Technologies with Hybrid Systems*, Proc. Natl. Acad. Sci. U.S.A. **112**, 3866 (2015).
[41] K. Stannigel, P. Komar, S. J. M. Habraken, S. D. Bennett, M. D. Lukin, P. Zoller, and P. Rabl, *Optomechanical Quantum Information Processing with Photons and Phonons*, Phys. Rev. Lett. **109**, 013603 (2012).
[42] M. Schmidt, M. Ludwig, and F. Marquardt, *Optomechanical Circuits for Nanomechanical Continuous Variable Quantum State Processing*, New J. Phys. **14**, 125005 (2012).
[43] M. Eichenfield, J. Chan, R. M. Camacho, K. J. Vahala, and O. Painter, *Optomechanical Crystals*, Nature (London) **462**, 78 (2009).
[44] M. Yuan, V. Singh, Y. M. Blanter, and G. A. Steele, *"Large Cooperativity and Microkelvin Cooling with a Three-Dimensional Optomechanical Cavity*, Nat. Commun. **6**, 8491 (2015).

Supplemental Material to "Low-noise amplification and frequency conversion with a multiport microwave optomechanical device"

C. F. Ockeloen-Korppi,[1] E. Damskägg,[1] J.-M. Pirkkalainen,[1] T. T. Heikkilä,[2] F. Massel,[2] and M. A. Sillanpää[1]

[1] *Department of Applied Physics, Aalto University, PO Box 11100, FI-00076 Aalto, Finland*
[2] *Department of Physics, Nanoscience Center, University of Jyväskylä, PO Box 35 (YFL), FI-40014 University of Jyväskylä, Finland*

(Dated: September 22, 2016)

THEORETICAL MODEL

In this section we provide some further details of the theoretical description of the system. In the laboratory frame, the Hamiltonian of the system is given by

$$H = \omega_1 a^\dagger a + \omega_2 c^\dagger c + \omega_m b^\dagger b + \left(g_1 a^\dagger a + g_2 c^\dagger c\right)(b^\dagger + b) \tag{S1}$$

where a and c represent the cavity modes for cavity 1 and 2 with resonant frequencies ω_1 and ω_2, while b ($b^\dagger$) is the lowering (raising) operator associated with the mechanical resonator, with resonant frequency ω_m. The coupling between the cavities and the mechanics is described in terms of radiation pressure interaction with coupling constants g_1 and g_2. We follow [1] and consider below the experimental situation where the pump frequencies satisfy $\omega_{P-} = \omega_2 - \omega_m$ and $\omega_{P+} = \omega_1 + \omega_m$. We then expand the cavity operators around the classical response. In the rotating frame with respect to cavity frequencies, the first quantum corrections are described by $H = H_0 + H_I$, where the uncoupled Hamiltonian is $H_0 = \omega_m(b^\dagger b + c^\dagger c - a^\dagger a)$. Retaining only the resonant terms in the remaining linearized interaction yields the coupling Hamiltonian

$$H_I = (G_- c^\dagger + G_+ a)b + h.c., \tag{S2}$$

where $G_- = g_2\sqrt{n_2}$, $G_+ = g_1\sqrt{n_1}$, and n_2 and n_1 are the photon numbers for the red-detuned and blue-detuned pumping tones for cavity 2 and 1, respectively. Applying the two-mode squeezing operator $S(\xi) = \exp\left[\xi c^\dagger a^\dagger - \xi c a\right]$, to the cavity operators

$$\begin{aligned}\eta_{\mathrm{A}} &= S^\dagger(\xi) c S(\xi) = \cosh\xi\, c + \sinh\xi\, a^\dagger \\ \eta_{\mathrm{B}} &= S^\dagger(\xi) a S(\xi) = \cosh\xi\, a + \sinh\xi\, c^\dagger,\end{aligned} \tag{S3}$$

the Hamiltonian H_I can be recast as a beam-splitter Hamiltonian

$$H_{\mathrm{I}} = \mathcal{G}\left(\eta_{\mathrm{A}} b^\dagger + \eta_{\mathrm{A}}^\dagger b\right), \tag{S4}$$

where we have defined

$$\cosh\xi = G_-/\mathcal{G}, \quad \sinh\xi = G_+/\mathcal{G} \quad \text{with } \mathcal{G}^2 = G_-^2 - G_+^2, \tag{S5}$$

with $G_- > G_+$. Note here how η_{B} is a mechanically dark mode (i.e. it does not couple to the mechanics). Assuming the standard dissipation mechanism for the cavities and the mechanics, with dissipation coefficients given by κ (equal for both cavities) and γ, the quantum Langevin equations for η_{A} and η_{B} can be solved to give [2]

$$\eta_{\mathrm{A}} = \frac{\chi_{\mathrm{m}}^{-1}}{\chi_{\mathrm{m}}^{-1}\chi_{\mathrm{c}}^{-1} + \mathcal{G}^2}\sqrt{\kappa}\eta_{\mathrm{A}} - \frac{i\mathcal{G}\sqrt{\gamma}}{\chi_{\mathrm{m}}^{-1}\chi_{\mathrm{c}}^{-1} + \mathcal{G}^2} b_{\mathrm{in}} \tag{S6}$$

$$\eta_{\mathrm{B}} = \chi_c\sqrt{\kappa}\cosh\xi\, a_{\mathrm{in}} + {\chi_c}^*\sqrt{\kappa}\sinh\xi\, c_{\mathrm{in}}^\dagger, \tag{S7}$$

where $\chi_{\mathrm{m}} = [\gamma/2 - i\omega]^{-1}$ and $\chi_{\mathrm{c}} = [\kappa/2 - i\omega]^{-1}$ are the bare mechanical and cavity responses in the rotating frame. Transforming η_{A} and η_{B} back to a and c,

$$\begin{aligned}a &= S(\xi) a S^\dagger(\xi) = \cosh\xi\, \eta_{\mathrm{B}} - \sinh\xi\, \eta_{\mathrm{A}}^\dagger \\ c &= S(\xi) c S^\dagger(\xi) = \cosh\xi\, \eta_{\mathrm{A}} - \sinh\xi\, \eta_{\mathrm{B}}^\dagger,\end{aligned} \tag{S8}$$

and, taking into account the input-output relations for the cavity fields [3],

$$\begin{aligned} a_{\rm out} + a_{\rm in} &= \sqrt{\kappa_{\rm e}}a \\ c_{\rm out} + c_{\rm in} &= \sqrt{\kappa_{\rm e}}c, \end{aligned} \tag{S9}$$

we can write the expression for the output fields a and c. It reads

$$\begin{aligned} a_{\rm out} = &(-\kappa_{\rm e}\mathcal{A}_{aa} - 1)a_{\rm in} - \kappa_{\rm e}\mathcal{A}_{ac}c_{\rm in}^{\dagger} \\ &- \sqrt{\kappa_{\rm i}\kappa_{\rm e}}\mathcal{A}_{aa}a_{I,\rm in} - \sqrt{\kappa_{\rm i}\kappa_{\rm e}}\mathcal{A}_{ac}c_{I,\rm in}^{\dagger} + i\sqrt{\gamma\kappa_{\rm e}}\frac{G_+}{(\chi_c\chi_m)^{-1} + \mathcal{G}^2}b_{\rm in}^{\dagger} \end{aligned} \tag{S10}$$

$$\begin{aligned} c_{\rm out} = &(\kappa_{\rm e}\mathcal{A}_{cc} - 1)c_{\rm in} + \kappa_{\rm e}\mathcal{A}_{ca}a_{\rm in}^{\dagger} \\ &+ \sqrt{\kappa_{\rm i}\kappa_{\rm e}}\mathcal{A}_{cc}c_{I,\rm in} + \sqrt{\kappa_{\rm i}\kappa_{\rm e}}\mathcal{A}_{ca}a_{I,\rm in}^{\dagger} - i\sqrt{\gamma\kappa_{\rm e}}\frac{G_-}{(\chi_c\chi_m)^{-1} + \mathcal{G}^2}b_{\rm in} \end{aligned} \tag{S11}$$

where

$$\begin{aligned} \mathcal{A}_{aa} &= (\chi_c^e \sinh^2\xi - \chi_c\cosh^2\xi)^* \\ \mathcal{A}_{cc} &= \chi_c^e\cosh^2\xi - \chi_c\sinh^2\xi \\ \mathcal{A}_{ca} = \mathcal{A}_{ac}^* &= (\chi_c^e - \chi_c)\cosh\xi\sinh\xi \end{aligned} \tag{S12}$$

and $\chi_c^e = \chi_{\rm c}\left(1 + \mathcal{G}^2\chi_{\rm c}\chi_{\rm m}\right)^{-1}$ represents the effective cavity response in the presence of the two-tone optomechanical drive. In eqs. (S10, S11), we have explicitly included the possibility of internal cavity losses (and noise) for both cavities by introducing the operators $a_{I,\rm in}$ and $c_{I,\rm in}$. From eqs. (S11, S12), one readily obtains the direct gain $A_{\rm d}$ and cross gain $A_{\rm x}$ for output field a,

$$\begin{aligned} A_{\rm d} &= -\kappa_{\rm e}\mathcal{A}_{aa} - 1 \\ A_{\rm x} &= -\kappa_{\rm e}\mathcal{A}_{ac}. \end{aligned} \tag{S13}$$

In the case of strong pumping $4G_-^2 \gg \gamma\kappa$, the maximum direct gain $A_{\rm d}$ can be written as

$$A_{\rm d}|_{\omega=0} \approx \frac{(8\frac{\kappa_e}{\kappa} - 4)G_-^2 + 4G_+^2 + \gamma\kappa}{4\mathcal{G}^2 + \gamma\kappa}. \tag{S14}$$

Assuming further $\mathcal{G}^2 \ll G_-^2$ (and hence $G_+ \simeq G_-$), the term -1 in eq. (S13) can be neglected, and the maximum gains become

$$A_{\rm d}|_{\omega=0} \approx 2\left[\frac{\kappa_e}{\kappa}\frac{4G_-^2/\kappa}{\gamma + 4\mathcal{G}^2/\kappa}\right], \quad A_{\rm x}|_{\omega=0} = 2\left[\frac{\kappa_e}{\kappa}\frac{4G_-G_+/\kappa}{\gamma + 4\mathcal{G}^2/\kappa}\right]. \tag{S15}$$

The bandwidth of amplification is given by the effective mechanical damping, given by

$$\gamma_{\rm eff} = \gamma + \frac{4\mathcal{G}^2}{\kappa}. \tag{S16}$$

When the bandwidth is determined by the optomechanical pumping, i.e., $4\mathcal{G}^2/\kappa \gg \gamma$, the expressions for the direct and cross-gains become particular simple,

$$A_{\rm d}|_{\omega=0} \overset{4\mathcal{G}^2 \gg \gamma\kappa}{\approx} 2\left[\frac{\kappa_e}{\kappa}\frac{1}{1-x^2}\right], \quad A_{\rm x}|_{\omega=0} \overset{4\mathcal{G}^2 \gg \gamma\kappa}{\approx} 2\left[\frac{\kappa_e}{\kappa}\frac{x^2}{1-x^2}\right], \tag{S17}$$

where $x = G_+/G_- \lesssim 1$.

From the expression of the output fields given by eq. (S10), the added noise at the output port of cavity 1, assuming direct amplification, can be written as

$$\begin{aligned} S_{\rm add,d} &= \frac{1}{2}\langle a_{\rm out}^{\dagger}a_{\rm out} + a_{\rm out}a_{\rm out}^{\dagger}\rangle - \frac{1}{2}\left|A_{\rm d}\right|^2\langle a_{\rm in}^{\dagger}a_{\rm in} + a_{\rm in}a_{\rm in}^{\dagger}\rangle \\ &= \kappa_{\rm i}\kappa_{\rm e}|\mathcal{A}_{aa}|^2\left(n_a^T + \frac{1}{2}\right) \\ &\quad + |\kappa_{\rm e}\mathcal{A}_{ac}|^2\left(n_c + \frac{1}{2}\right) + \kappa_{\rm i}\kappa_{\rm e}|\mathcal{A}_{ac}|^2\left(n_c^T + \frac{1}{2}\right) \\ &\quad + \frac{\gamma\kappa_{\rm e}G_+^2}{|(\chi_c\chi_m)^{-1} + \mathcal{G}^2|^2}\left(n_m^T + \frac{1}{2}\right) \end{aligned} \tag{S18}$$

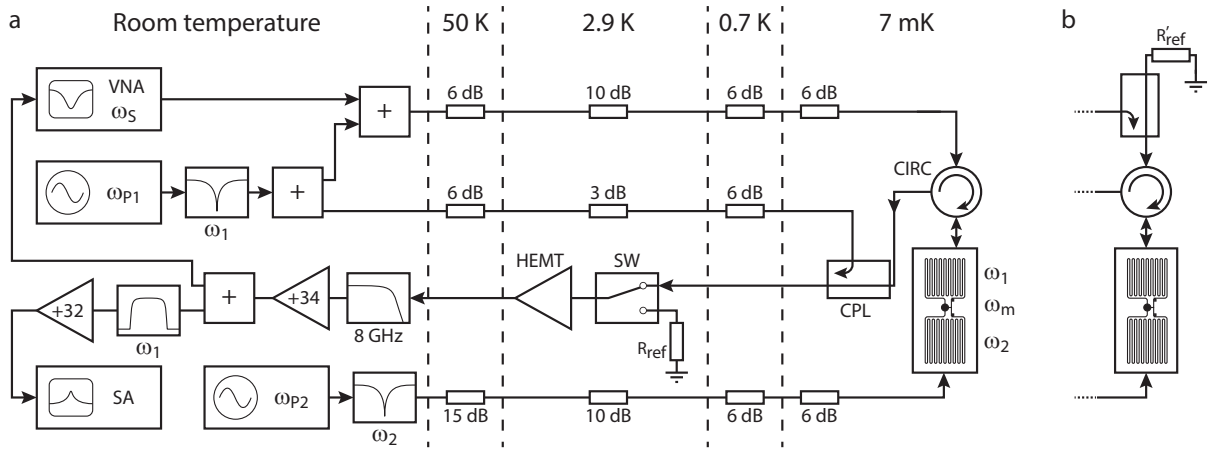

Figure S1. Measurement setup and cryogenic temperature stages. a) Main setup. Shown are network analyzer (VNA), signal generators ($\omega_{\rm P1}$, $\omega_{\rm P1}$), signal analyzer (SA), power splitters / combiners (+), circulators (CIRC), directional coupler (CPL), switch (SW), noise source $\rm R_{ref}$, HEMT amplifier, filters, attenuators and room-temperature amplifiers. b) Alternative low-temperature setup used in a separate calibration cooldown.

while for cross-amplification we have

$$\begin{aligned} S_{\rm add,x} &= \frac{1}{2}\langle a_{\rm out}^\dagger a_{\rm out} + a_{\rm out} a_{\rm out}^\dagger\rangle - \frac{1}{2}|A_{\rm x}|^2\,\langle c_{\rm in}^\dagger c_{\rm in} + c_{\rm in} c_{\rm in}^\dagger\rangle \\ &= |-\kappa_{\rm e}\mathcal{A}_{aa} - 1|^2\left(n_a + \frac{1}{2}\right) + \kappa_{\rm i}\kappa_{\rm e}|\mathcal{A}_{aa}|^2\left(n_a^T + \frac{1}{2}\right) \\ &\quad + \kappa_{\rm i}\kappa_{\rm e}|\mathcal{A}_{ac}|^2\left(n_c^T + \frac{1}{2}\right) \\ &\quad + \frac{\gamma\kappa_{\rm e}G_+^2}{|(\chi_c\chi_m)^{-1} + \mathcal{G}^2|^2}\left(n_m^T + \frac{1}{2}\right), \end{aligned} \tag{S19}$$

and analogous expressions hold for cavity 2. Here, n_a^T, n_c^T, and n_m^T are the bath temperatures of cavity 1, cavity 2, and the mechanics, respectively, expressed as number of quanta. The occupation numbers n_a and n_c correspond to the $a_{\rm in}$ and $c_{\rm in}$, respectively. From eqs. (S19) and (S20) in the large-gain limit ($G_- \simeq G_+$) and for small internal losses ($\kappa_{\rm e} \gg \kappa_{\rm i}, \gamma$), both $S_{\rm add,d}$ and $S_{\rm add,x}$ approach the quantum limit ($S_{\rm add,d}/|A_{\rm d}|^2 \simeq S_{\rm add,x}/|A_{\rm x}|^2 \gtrsim 1/2$).

It is interesting to note how the contribution from the mechanical resonator bath is reduced in this scheme compared to the amplification with only blue-detuned cavity driving [2]. Namely, for a signal on resonance ($\omega = 0$), and for $4\mathcal{G}^2 \gg \kappa\gamma$ the equivalent added noise from the mechanical bath (last lines on eqs. (S17) and (S18)) is

$$S_{\rm add,m}/|A_{\rm d}|^2 = \frac{\gamma\kappa^2 G_+^2}{4\kappa_e G_-^4}\left(n_m^T + \frac{1}{2}\right). \tag{S20}$$

For cross-amplification this result is further multiplied by G_-^2/G_+^2. These results mean that near-quantum limited amplification is possible even when the bath of the mechanical resonator responsible for the non-linear interaction is not very close to its ground state.

EXPERIMENTAL SETUP

Our measurement setup is shown in figure S1a. We use a Bluefors dry dilution refrigirator to cool the sample to a base temperature of 7 mK. The input lines are attenuated at each temperature stage to prevent thermal noise from reaching the sample, so that the sample sees essentially only vacuum noise at its inputs.

The two pump tones, here labelled $\omega_{\rm P1}$ and $\omega_{\rm P2}$, are generated by Anritsu MG3692C signal generators, and passed through a notch filter tuned to ω_1 and ω_2, respectively, to prevent generator phase noise from coupling to the cavities, and injected into cavity 1 and 2, respectively. The probe tone at ω_s is generated by a R&S ZVA40 vector network

analyzer (VNA) is combined with either probe ω_{P1} (shown) or ω_{P2}, depending on the measurement. All signal generators and analyzers are frequency locked to the same reference.

The output signal of cavity 1 is separated from the input by a circulator, and pre-amplified by a HEMT amplifier (LNF-LNC4_8A) at 2.9 K. To avoid saturating the HEMT amplifier, we add part of the pump signal to the sample output using a directional coupler, carefully adjusted to cause negative interference with the pump signal that was reflected off the sample. At the input of the HEMT amplifier, a mechanical switch can switch in a thermal noise source at 2.9 K to give an absolute calibration of the output power (described below).

The output signal is further amplified at room temperature, and split to the input of the VNA and of a Anritsu MS2830A signal analyzer (SA). The SA input signal is first passed through a filter with a pass-band of a few MHz around ω_1, in order to further reduce the amplitude of the pump tone ω_{P1}.

We also use the VNA to measure the line shape of cavity 1 in a reflection measurement. To establish a reference of the background reflection due to the tranmission lines and filters, we fit a polynomial to the magnitude data outside the cavity resonance. We then divide the complex reflection data by this fit, and extract $\kappa_{\mathrm{int}} = 2\pi \times (0.50 \pm 0.05)$ MHz and $\kappa_{\mathrm{ext}} = 2\pi \times (4.8 \pm 0.2)$ MHz from the resulting amplitude and phase data. The background fit is also used to calibrate the amplifier gain, assuming a gain of 1 (perfect reflection) off resonance from the cavity. A direct measurement of cavity 2 was not possible in the experiment, as the output of cavity 2 was not measured. From the circuit geometry and fabrication uncertainties, we expect the cavity linewidths to be similar within about a factor 1.5. We have verified numerically that such differences do not affect the expected gain profiles and added noise. Hence, for plotting theory curves, we assume cavity 2 to have the same line width as cavity 1.

Calibration of output noise and system gain

A precise calibration of the power at the output of the sample is crucial for our measurements. We perform this calibration by comparing to a known noise source $\mathrm{R_{ref}}$. We first turn off all pump and probe tones and measure the vacuum noise originating from the mK stage. At the signal analyzer (SA), this results in a noise power spectral density (PSD) of $S_0 = (\frac{1}{2} + S_{\mathrm{H}})A_{\mathrm{H}}^2$, expressed in number of quanta (multiplication by $\hbar\omega$ gives power per unit bandwidth). Here, S_{H} is the effective noise added by the cryogenic HEMT amplifier, and A_{H}^2 is the total power gain from the input of the HEMT to the SA. Then, we flip switch SW and measure the reference noise $S_1 = (S_{\mathrm{ref}} + S_{\mathrm{H}})A_{\mathrm{H}}^2$, where $S_{\mathrm{ref}} = 8.67$ is the thermal noise of resistor $\mathrm{R_{ref}}$ at a measured temperature of 2.91 K. By comparing these measurements, we find $S_{\mathrm{H}} = 17.6 \pm 1.3$ and $A_{\mathrm{H}}^2 = (75.7 \pm 0.3)$ dB.

In a typical measurement, we wish to measure the output PSD of the sample, S_{out}, which results in $S_{\mathrm{SA}} = (\alpha S_{\mathrm{out}} + S_{\mathrm{H}})A_{\mathrm{H}}^2$ at the SA. Here, α accounts for any attenuation between the sample and the HEMT amplifier. We estimate $\alpha = -1.5 \pm 1.0$ dB based on the low-temperature cabling. In the main text, we plot the effective output PSD,

$$S_{\mathrm{out,eff}} = \frac{S_{\mathrm{SA}}}{\alpha A_{\mathrm{H}}^2}, \tag{S21}$$

which is equal to S_{out} plus technical noise. In noise measurements we plot the effective input noise PSD, referred to the input of cavity 1,

$$S_{\mathrm{in,eff}} = \frac{S_{\mathrm{SA}}}{\alpha A_{\mathrm{H}}^2 A_{\mathrm{d}}^2}, \tag{S22}$$

where A_{d} is the direct gain of the mechanical amplifier, measured independently. We emphasize that the quantities (S21, S22) characterize the total system performance, including the added noise of all further amplification stages. The total calibration uncertainty in (S21) and (S22) is 1.0 dB, dominated by the uncertainty in α.

The theory curves in figure 2 of the main text include the quantum noise of the input, the predicted added noise of the mechanical amplifier (equation S19), as well as the effective HEMT noise, and is calculated as

$$S_{\mathrm{in,eff}} = \frac{1}{2} + S_{\mathrm{add,d}} + \frac{S_{\mathrm{H,eff}}}{A_{\mathrm{d}}^2}, \tag{S23}$$

where A_x is the the predicted cross gain of the mechanical amplifier and $S_{\mathrm{H,eff}} = S_{\mathrm{H}}/\alpha$ the effective technical noise of the HEMT amplifier as well as any further amplification stages.

To verify the calibration of α, we performed a second cooldown where the reference noise source is at the sample input, as shown in figure S1b. The noisy resistor R'_{ref} is connected to the sample input, and the input signal and pump

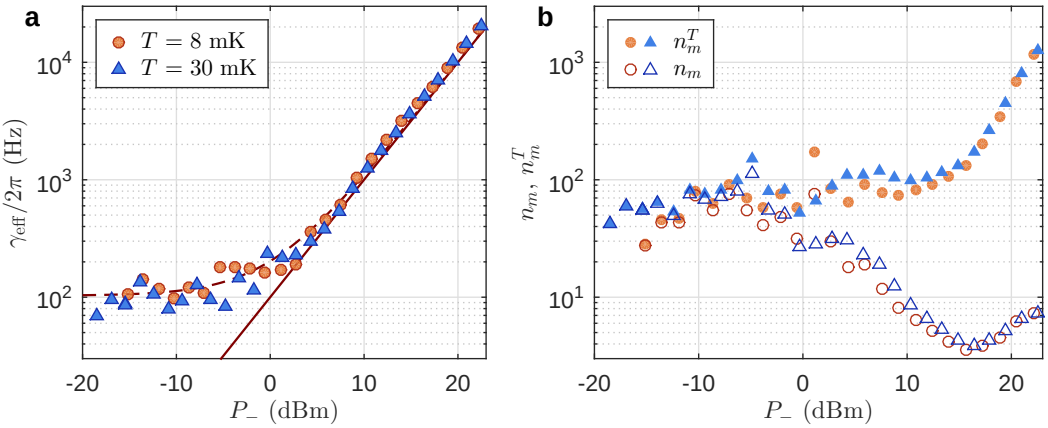

Figure S2. Optomechanical cooling. a) Total linewidth $\gamma_{\rm eff}$ obtained from fits of the output spectrum to equation (S25) at a fridge temperature of 8 mK (circles) and 30 mK (triangles), as a function of pump power. The dashed and solid lines show the fitted $\gamma_{\rm eff}$ and $\gamma_{\rm opt} \propto P_-$, respectively. b) Mechanical mode occupation n_m and mechanical bath temperature n_m^T extracted from the fits, expressed as number of quanta, showing optomechanical cooling down to $n_{m,\rm min} = 3.4$ quanta.

are combined with it on a -20 dB directional coupler. The noise resistor has an independent heater and temperature sensor, and we vary its temperature to create a calibrated variable noise source $S_{\rm ref}(T)$. We measure the PSD at the SA, which is epxected to follow

$$S_{\rm SA}(T) = \left(S_{\rm ref}(T)A_{\rm d}^2 + S_{\rm H,eff}\right)\alpha A_{\rm H}^2. \tag{S24}$$

Off cavity resonance ($A_{\rm d}^2 = 1$), a fit to equation (S24) alows us to extract $S_{\rm H,eff}$ independently of α and $A_{\rm H}$. We find $S_{\rm H,eff} = 24$, in excellent agreement with the main calibration described above ($\alpha S_{\rm H} = 25$). With the pumps enabled, and measuring on cavity resonance, equation (S24) also allows us to directly measure the amplifier added noise. However, due to the additional directional coupler in this cooldown the pump power available at the sample was limited to $G_+ \approx G_- \approx 2\pi \times 60$ kHz. At this power, we find $S_{\rm add,d} = 6$ quanta, in good agreement with the values reported figure 3c of the main text.

Optomechanical cooling

To calibrate the thermal bath temperature of the mechanical oscillator, we perform a series of standard optomechanical cooling measurements. Here, we use a single pump at the lower (red) mechanical side-band co-resonance of cavity 1. The output spectrum at frequency $\delta = (\omega - \omega_1) \ll \kappa, \omega_m$ has a Lorentzian form [4]

$$S_{\rm out}(\delta) = \frac{4\kappa_{\rm e}}{\kappa} n_a^T + \gamma_{\rm opt}\frac{\kappa_{\rm e}}{\kappa}\frac{\gamma_{\rm eff}}{\delta^2 + \gamma_{\rm eff}^2/4}\left(n_m - 2n_a^T\right), \tag{S25}$$

where $\gamma_{\rm eff} = \gamma(T) + \gamma_{\rm opt}$ is the total mechanical line width, $\gamma_{\rm opt}$ the opto-mechanical cooling rate (see eq. (8) in ref. [5]), n_m the occupation of the mechanical mode, and n_m^T and n_a^T the bath temperature of the mechanics and cavity 1, respectively, expressed in number of quanta.

We first calibrate the intrinsic mechanical linewidth $\gamma = 2\pi \times (103 \pm 20)$ Hz from measurements at low pump power and low cryostat temperature T, where $\gamma_{\rm eff} \approx \gamma$. Then, we measure the output spectrum as function of pump power P_-. We perform the measurements at two temperatures, 8 mK and 30 mK, both in the low-T limit where $\gamma(T) \approx \gamma$. Using the calibrated total system gain from eq. (S21), we can directly fit eq. (S25) to the data and extract the quantities $\gamma_{\rm eff}$, n_a^T, and $\gamma_{\rm opt}(n_m - 2n_a^T)$, corresponding to line width, offset and peak area of the Lorentzian, respectively. The fit results show $n_a^T \ll 1$ for all measured powers.

Figure S2a shows the extracted $\gamma_{\rm eff}$ versus P_-. Here, the P_- is the output power of the microwave generator. At high powers, $\gamma_{\rm eff}$ is dominated by $\gamma_{\rm opt} \propto P_-$, and we extract the proportionality coefficient from a fit to this data (solid line in figure S2a). Using the now calibrated $\gamma_{\rm opt}$, we caculate n_m from eq. (S25) and n_m^T from the relation [4]

$$n_m^T = \frac{\gamma(T) + \gamma_{\rm opt}}{\gamma(T)} n_m, \tag{S26}$$

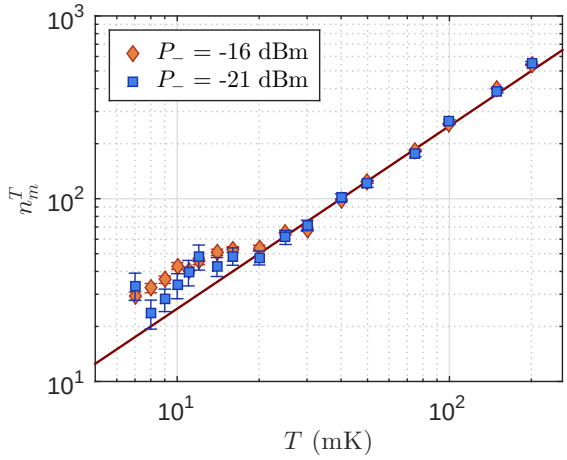

Figure S3. Mechanical oscillator thermalization. Measured mechanical bath temperature n_m^T as a function of cryostat temperature at low cooling power. The mechanical oscillator thermalizes down to 20 mK. The solid line shows the expected thermal occupation. Error bars indicate statistical uncertainty (68% confidence intervals).

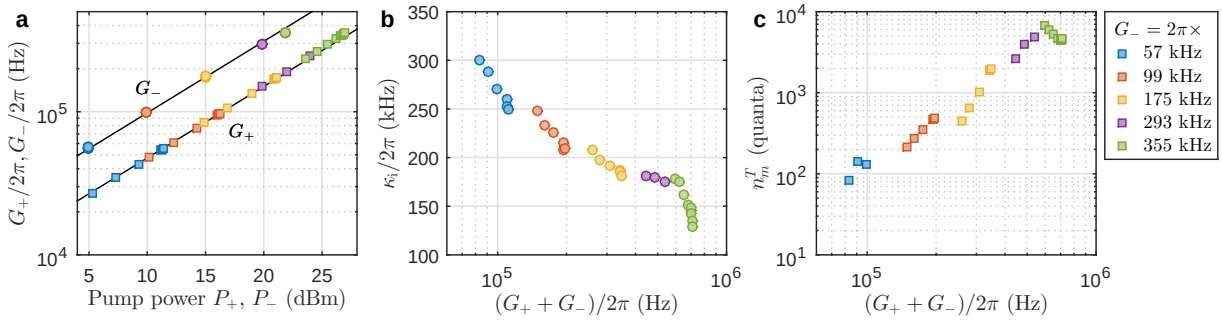

Figure S4. Fit results for two-port amplifier measurements. a) Fitted G_- (circles) and G_+ (squares) as function of pump power at the generator. Solid lines show the expected scaling $G_\pm^2 \propto P_\pm$. b) Fitted internal cavity linewidth κ_i, showing a sharp decrease at the highest pump powers. c) Thermal environment of the mechanical oscillator, expressed as effective number of quanta. In all panels, data with the same color was taken with the same value of G_-, as indicated on the legend.

which holds for $\gamma_{\rm opt} \ll \kappa \ll 4\omega_m$ and $n_a^T \ll 1$. The results are shown in figure S2. At low pump powers, the mechanical mode is thermalized with the bath. As P_- increases, the mechanical mode is optomechanically cooled, down to $n_{m,\rm min} = 3.4$ quanta. For higher power, cooling is limited by heating of the environment as $n_m^T \propto P_-^2$ up to $n_m^T \approx 10^3$ for the highest pump powers used in our experiments.

Next, we measure the thermalization between the mechanical bath and the cryostat. We perform again a measurement with a single red-sideband pump, but using low power P_- and varying the temperature of the cryostat. Figure S3 shows n_m^T extracted from fits to eq. (S25), using $\gamma_{\rm opt}$ calibrated by the data in figure S2a. The data shows that the mechanical mode thermalizes down to 20 mK, showing good agreement with the expected $n_m^T = k_B T/\hbar\omega_m$ (solid line) above this temperature. This agreement also confirms the calibration of the total system gain $\alpha A_{\rm H}^2$.

DATA ANALYSIS AND ADDITIONAL DATA

Two-port amplifier

We measure the direct gain of our amplifier by injecting a weak signal into cavity 1, and recording the resulting reflection spectrum with the VNA. The gain is calibrated by assuming $|A_{\rm d}|^2 = 1$ outside the cavity resonance. We then record the output noise $S_{\rm out,eff}$ for the same pump powers but no input signal on the SA, immediately following the gain measurement to avoid any drifts in the gain profile. The input noise $S_{\rm in,eff} = S_{\rm out,eff}/|A_{\rm d}|^2$ is then calculated directly from the data.

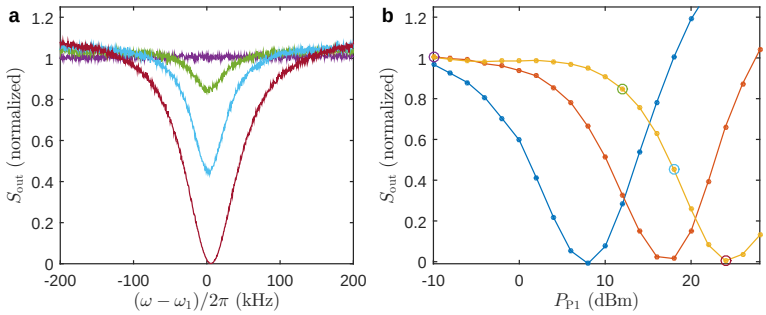

Figure S5. Frequency conversion from cavity 1 to cavity 2. a) Reflection spectrum $S(\omega)$ of cavity 1 (normalized) for $P_{\rm P2} = 28$ dBm (at the signal generator) and several powers $P_{\rm P1}$, showing a strong dip when the signal is converted to cavity 2. b) Value of $S(\omega)$ at the dip or peak, for a range of pump powers. Circles indicate the data shown in panel a.

To compare our results to theory, we fit the measured direct gain $|A_{\rm d}|$ to equation (S13) using G_-, G_+ and $\kappa_{\rm i}$ as free parameters. In addition, we allow for a $\mathcal{O}$(kHz) frequency shift arising from the radiation pressure force of the pumps. Figure S4a,b shows the results of the fit. We find the coupling strengths $G_\pm^2$ are in excellent agreement with the expected scaling proportional to pump power $P_\pm$. The internal cavity linewidth $\kappa_{\rm i}$ decreases significantly at high pump powers, which is a common effect observed in superconducting circuits and attributed to saturation of two-level systems in the substrate, reducing the effective loss channels.

We then compare our measured noise data $S_{\rm in,eff}$ to the expected theory calculated with equation (S23), where $S_{\rm add}$ is calculated with the parameters obtained from the gain fit. In accordance with the optomechanical cooling measurements discussed in the previous section, we assume $n_a^T = n_c^T \approx 0$, and adjust n_m^T. We find that the theory describes the data well for all pump powers with the values for n_m^T shown in figure S4c. The scaling, n_m^T scales approximately with P_+^2, and the magnitude is consistent with that observed in figure S2b at high pump powers. At the highest values of P_+ the scaling is reduced, which may be related to the steeper decrease in $\kappa_{\rm i}$ observed at those powers (figure S4b).

As discussed in the main text, the amplifier can be tuned within the cavity line width κ by shifting the pump frequencies in unison. We find the highest gain is obtained slightly away from the cavity center of the resonance dip observed in reflection measurements. We therefore assume this optimum point to be the true value of ω_1 in the presence of pumping. Similarly, we find the value of ω_2 (which cannot be measured directly in our setup) by maximizing the gain obtained in the two-port amplifier.

Frequency conversion without amplification

Here we show additional data of frequency conversion without amplification, using the pump scheme depicted in figure 4b in the main text. Figure S5 shows frequency conversion from cavity 1 to cavity 2. The reflected signal of cavity 1 is shown for several pump powers, normalized to unity reflection with all pumps off. As the signal is frequency-converted to cavity 2, a dip is visible in the reflection signal. For balanced pump powers, we observe an attenuation of the signal by 29 dB.

[1] Y.-D. Wang and A. A. Clerk, "Reservoir-engineered entanglement in optomechanical systems," Phys. Rev. Lett. **110**, 253601 (2013).

[2] F. Massel, T. T. Heikkilä, J.-M. Pirkkalainen, S. U. Cho, H. Saloniemi, P. J. Hakonen, and M. A. Sillanpää, "Microwave amplification with nanomechanical resonators," Nature **480**, 351–354 (2011).

[3] D.F. Walls and Gerard J. Milburn, eds., *Quantum Optics* (Springer-Verlag, Berlin Heidelberg, 2008).

[4] T Rocheleau, T Ndukum, C Macklin, JB Hertzberg, AA Clerk, and KC Schwab, "Preparation and detection of a mechanical resonator near the ground state of motion," Nature **463**, 72–75 (2010).

[5] Florian Marquardt, Joe P. Chen, A. A. Clerk, and S. M. Girvin, "Quantum theory of cavity-assisted sideband cooling of mechanical motion," Phys. Rev. Lett. **99**, 093902 (2007).